ACS Photonics

Article

pubs.acs.org/journal/apchd5

Near-Infrared Photodetector Based on MoS_2/Black Phosphorus Heterojunction

Lei Ye,[†,‡,∥] Hao Li,[†,∥] Zefeng Chen,[†] and Jianbin Xu*[,†,§]

[†]Department of Electronic Engineering, Materials Science and Technology Research Center, The Chinese University of Hong Kong, Shatin, New Territories, Hong Kong, People's Republic of China

[‡]School of Optical and Electronic Information, Huazhong University of Science and Technology, 1037 Luoyu Road, Wuha, Hubei 430074, People's Republic of China

[§]Materials Science and Technology Research Center, The Chinese University of Hong Kong, Shatin, New Territories, Hong Kong SAR, People's Republic of China

Supporting Information

ABSTRACT: Two-dimensional (2D) materials present their excellent properties in electronic and optoelectronic applications, including in ultrafast carrier dynamics, layer-dependent energy bandgap, tunable optical properties, low power dissipation, high mobility, transparency, flexibility, and the ability to confine electromagnetic energy to extremely small volumes. Herein, we demonstrate a photodetector with visible to near-infrared detection range, based on the heterojunction fabricated by van der Waals assembly between few-layer black phosphorus (BP) and few-layer molybdenum disulfide (MoS_2). The heterojunction with electrical characteristics which can be electrically tuned by a gate voltage achieves a wide range of current-rectifying behavior with a forward-to-reverse bias current ratio exceeding 10^3. The photoresponsivity (R) of the photodetector is about 22.3 A W^{-1} measured at λ = 532 nm and 153.4 mA W^{-1} at λ = 1.55 μm with a microsecond response speed (15 μs). In addition, its specific detectivity D^* is calculated to have the maximum values of 3.1 × 10^{11} Jones at λ = 532 nm, while 2.13 × 10^9 Jones at λ = 1550 nm at room temperature.

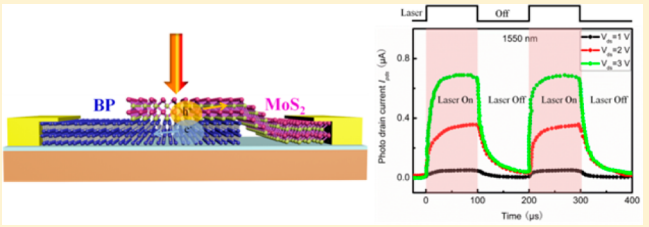

KEYWORDS: *two-dimensional materials, optoelectronics, vertical diode, gate-tunable modulation, photovoltaic*

Photodetectors have significant importance in modern society from practical aspects like imaging, communication devices, various sensors for safety monitoring, and display technology to fundamental science applications.[1−5] At present, various commercial photodectors with mature process technology are mostly based on silicon, crystalline InGeAs/HgCdTe, or other inorganic semiconductor materials, but the blemishes of these photodetectors are also obvious, such as that silicon-based photodetectors are limited to the visible region due to silicon's band gap corresponding to wavelength of ∼900 nm, and long wavelength photodetector products based on crystalline InGeAs/HgCdTe suffer from either expensive fabricating process (e.g., molecular beam epitaxy) or rigorous operation demands (e.g., low temperature), sometimes both, and so on. Recently, two-dimensional (2D) nanomaterials applied in photodetectors have attracted great attention due to their unique optoelectronic properties,[6−9] and the easy integration between 2D materials in complex structures, which are free of the traditional lattice mismatch issue.[10,11] Among 2D materials, MoS_2 has shown its good properties in optoelectronic applications, especially in photodetectors.[12−15] However, MoS_2 photodetectors only respond to the visible region, leading to limitation of their applicable scope, especially for the important applications of the infrared region.[12,16] To circumvent the weakness, a promising approach is to create multifunctional hybrid photodetectors based on crystal heterogeneous stacks built by different two-dimensional materials, because the availability of 2D materials with different bandgaps and workfunctions allows bandgap engineering of heterostructures.[17] Furthermore, the ability to electrostatically tune carrier densities and band alignments of 2D materials offers an alternative way to devise novel heterostructures with various functionalities.[18−21] The formation of analogous heterojunctions between different two-dimensional (2D) materials would be possible via viable band engineering to open up new realms in the application of photodetectors under facile operation demands.

Here, we demonstrate a vertically integrated photodetector composed of a black phosphorus (BP)/molybdenum disulfide (MoS_2) van der Waals heterostructure, in which BP covering from the visible to the mid-infrared spectral range suggests that it is an ideal 2D material for potential applications in optoelectronics, especially in infrared region applications,[22,23] as shown in Figure 1a. The heterojunction displays the good gate-tunable modulation, which demonstrates a wide range of current-rectifying characteristics with forward-to-reverse bias

Received: February 2, 2016
Published: March 4, 2016

© 2016 American Chemical Society

DOI: 10.1021/acsphotonics.6b00079
ACS Photonics 2016, 3, 692−699

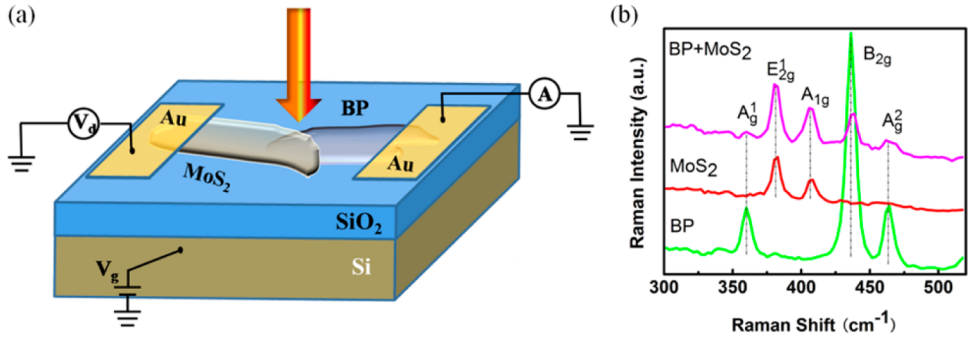

Figure 1. (a) Schematic of the BP/MoS_2 heterojunction. A p+ silicon wafer capped with 300 nm SiO_2 was used as the global back gate and the gate dielectric, respectively. Few-layer MoS_2 sheet was transferred onto few-layer black phosphorus sheet in order to form a van der Waals heterojunction. 100 nm thick gold films were tipped up and then aligned to the heterojunction as the electrodes. During the electrical measurements, a bias voltage V_{ds} was applied across the junction. The gate voltage V_g was applied to the back gate. (b) Raman spectra of the black phosphorus, MoS_2, and the overlapped regions. Characteristic Raman peaks of both the black phosphorus and MoS_2 sheets can be observed in the overlapped region.

current ratio exceeding 10^3. Furthermore, the photodetector responds to visible light of λ = 532 nm with the photoresponsivity of 22.3 A W^{-1} and to near-infrared light of λ = 1.55 μm with the photoresponsivity of 153.4 mA W^{-1}, and shows a microsecond response speed (15 μs) which is 2 to 3 orders of magnitude higher than those previously reported for few-layer BP phototransistors.[20,24] Moreover, the specific detectivity D^* of the detector is found to have the value of 2.13×10^9 Jones at 1550 nm wavelength under room temperature.

RESULTS AND DISCUSSION

The current generated by a bias voltage (V_{ds}) applied across the two electrodes flows through the BP/MoS_2 heterojunction channel, which can be modulated by a voltage (V_g) applied to the p+ doped silicon as the back gate, as shown in the device architecture (Figure 1a). All the following analyses and results were based on this specific device unless otherwise specified. The Raman spectra (Figure 1b) from the BP, MoS_2, and the heterojunction regions are presented in Figure 1b. The observed Raman-active modes of BP and MoS_2 are consistent with previously reported data.[25,26] Moreover, Raman spectrum of the BP/MoS_2 heterostructure in the overlapped region appears to comprise the addition of Raman modes from the two constituent layers, indicating good quality of thin flakes in the junction region after layer exfoliation and device fabrication. The top view of the BP/MoS_2 heterostructure can be visually observed by scanning electron microscope (SEM), showing the heterojunction between BP and MoS_2 with the small overlap region as the channel, as illustrated in the Supporting Information (Figure S1). In order to better show the vivid details about the heterojunction, the SEM EDX mapping of the junction was provided to demonstrate the structural composition of the junction. As shown in Figure S2, the junction is composed of the few-layer MoS_2 marked as purple, placed on the few-layer BP sheet denoted in green. The elemental analysis was also carried out by EDX mapping, as shown by Figure S3 and Figure S4). They clearly show P, Mo, and S elements in the junction, respectively, in accordance with the shape of each part of the junction. Particularly, the irregular Ga particles distributed on the device marked as azure are caused by Ga−In alloy which was used to paste the gold electrode. The surface morphology of the junction was also measured by atomic force microscope (AFM), as shown in Figure S5. The thicknesses of the few-layer black phosphorus flake and few-layer MoS_2 were ~22 and ~12 nm, respectively.

In this work, electrical characteristic studies of the BP/MoS_2 heterostructure were carried out. We first studied the $I-V$ characteristics, which are displayed on linear and log plots, as shown in Figure 2a. The observed $I-V$ characteristics look similar to those of the conventional p−n junction diode, and its forward characteristics present an ideality factor of ~2 at a low bias voltage, which was extracted from the $I-V$ curve using the method from the reference in low voltage regime.[27] Because of the certain thickness of BP and MoS_2, the depletion region of the junction is considered to cross the overlapped layers in the vertical direction.[28,29] The schematic and band diagrams of the junction at 0 bias, forward bias, and reverse bias are shown in Figure 2d, respectively. When the junction is under 0 bias, the charges generated by illumination are separated at the overlapped region. Under forward bias, the majority carriers in MoS_2 overcome the barrier to cross the junction, so the current increases with the increase of forward bias. Under reverse bias, the barrier increases and blocks the majority carriers. Although minority carriers are extracted to the other side of the junction, the low concentration of minority carriers results in the current being much lower than in forward bias, which generates the current-rectifying characteristics of the junction.

Figure 2b shows the $I-V$ curves of the junction at various gate voltages, as measured between the metal electrodes on BP (D) and MoS_2 (S) sheets, respectively. The gate-voltage-tuned rectification of current can be observed, as the electrostatic doping modulates the densities of free electrons and holes in the junction. The forward current can be increased by decreasing the back gate voltage, while the reverse current can be increased by increasing the back gate voltage, which is consistent with the reported work of Tobin J. Marks on the gate-tunable p−n diode.[30] As the gate voltage reduces, the rectification of the device increases, and the device transitions from a poorly rectifying state at V_g = 60 V to a highly rectifying state at V_g = −60 V. These results can be explained by a model describing the current transport of the p−n diode. As shown in Figure 2d, under forward bias, the majority carriers in MoS_2 increase under negative gate modulation leading to increasing the current, and the majority carriers in MoS_2 under positive gate modulated decrease to reduce the current. For reverse bias, the increased majority carriers in MoS_2 under negative gate modulation cannot cross the barrier and prevent the minority carriers from crossing the junction, resulting in the decrease of the current, but under positive gate modulation, the decrease of

DOI: 10.1021/acsphotonics.6b00079
ACS Photonics 2016, 3, 692−699

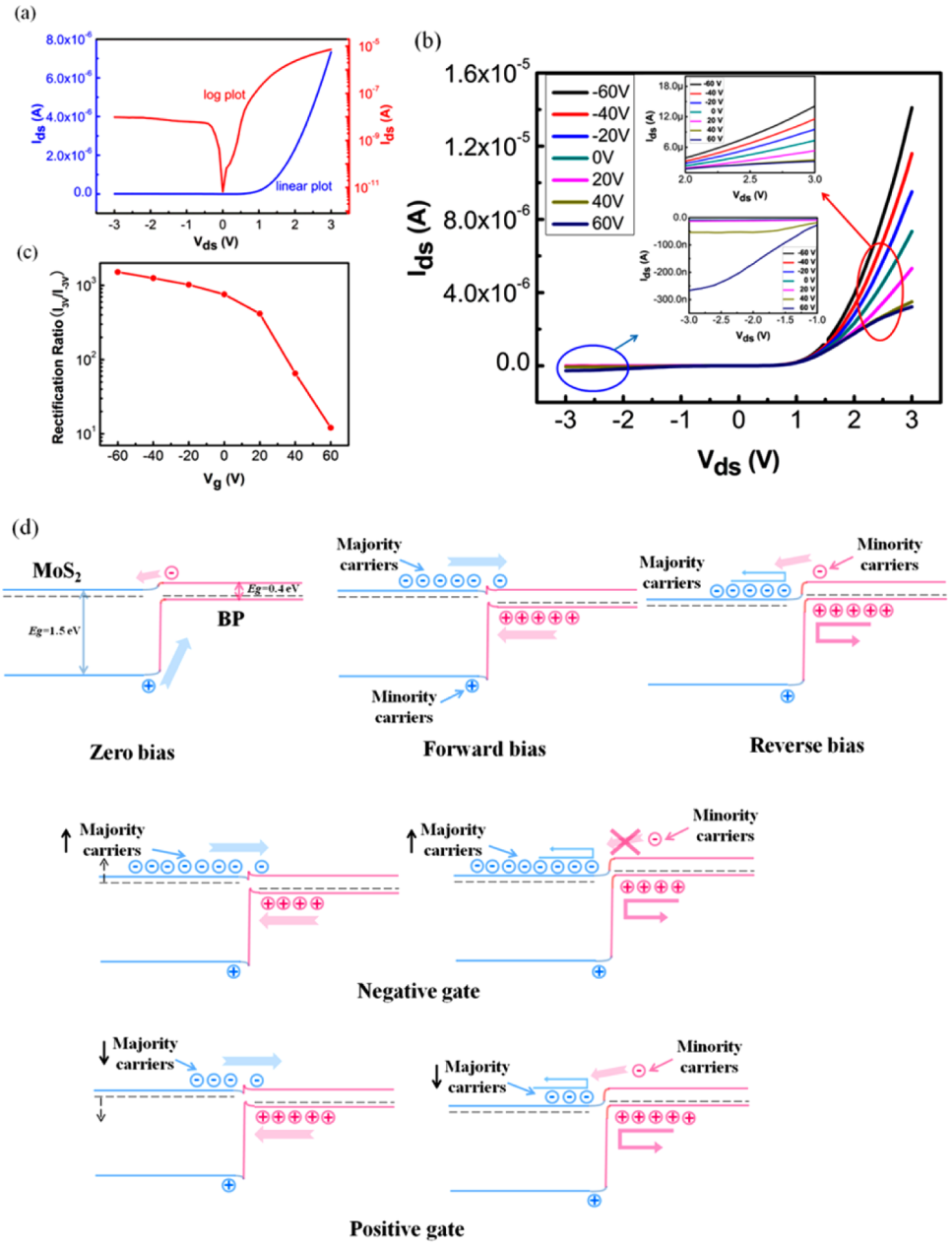

Figure 2. (a) The linear and log plots of $I-V$ characteristics of the BP/MoS_2 vertical heterojunction. (b) Gate tunable $I-V$ characteristics. The top inset shows gate tunable $I-V$ characteristics from V_{ds} = 2 V to V_{ds} = 3 V, and the bottom inset shows that from V_{ds} = −3 V to V_{ds} = −1 V. (c) The rectification ratio ($I_{Vds=3V}/I_{Vds=-3V}$) as a function of back gate voltage V_g. (d) The schematic and band diagrams of the junction under 0 bias, forward bias, reverse bias, negative gate modulation, and positive gate modulation.

major carriers in MoS_2 helps to extract minority carriers across the junction, leading to the increase of the current.

To further demonstrate the current-rectifying behavior of the junction, the relationship of the ratio between forward and reverse currents (under V_{ds} = 3/−3 V) and applied gate voltage (V_g) is plotted in Figure 2c. In contrast to the decrease of gate voltage, the ratio increases and goes to 1.5×10^3 at the gate bias of V_g = −60 V. The current-rectifying characteristics come from the interface region, which may be modeled as many parallel heterojunction diodes.

Based on the signatures of bound excitonic states in their absorption spectra for BP and MoS_2,[31,32] the photocurrent generation is expected on the heterojunctions under optical irradiation based on these materials. The BP/MoS_2 heterojunction was illuminated with a green laser (wavelength of 532 nm) at different photoexcitation intensities. The strong photoresponse of the junction is observed from $I-V$ characteristics under different incident laser powers, as shown in Figure 3a, indicating that the spontaneous charge separation occurred at the junction. In addition, the differences in the $I-V$ results can also be viewed by plotting the current versus voltage (I_{ds} vs V_{ds}) on logarithmic scale, as shown in the inset of Figure 3a. The current relation to bias voltage shows the marked increase under illumination, indicating that the junction has an active photoresponse. Moreover, in comparison with the behavior of solar cell devices, the junction under illumination demonstrates a distinct shift of voltage defined as V_{OC} (open circuit voltage) at which the absolute value of current becomes the minimum.

DOI: 10.1021/acsphotonics.6b00079
ACS Photonics 2016, 3, 692−699

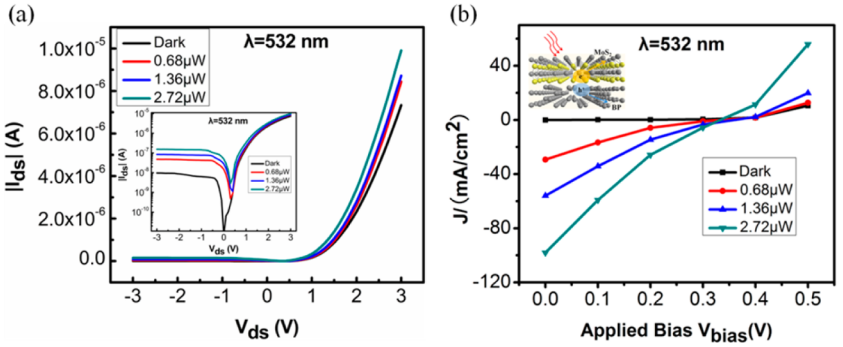

Figure 3. (a) $I-V$ characteristics of the BP/MoS_2 junction under illumination by 532 nm laser with various incident powers. The inset shows the log plots of these $I-V$ characteristics. (b) The relationships between the current density and applied voltage of the junction under illumination by 532 nm laser with various incident powers, showing the obvious photovoltaic properties. The inset shows the separation process of an optically excited exciton occurrence at the heterojunction.

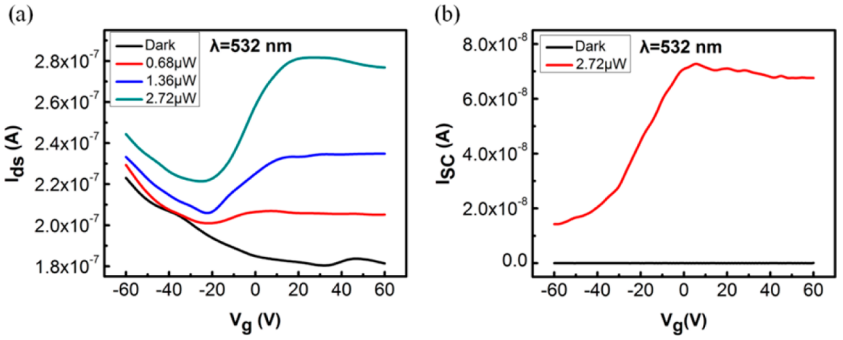

Figure 4. (a) The transfer curves ($I-V_g$) of the junction under illumination of 532 nm laser with a series of incident intensities, at V_{ds} = 1 V. (b) The comparison of the short-circuit current (I_{SC}) between the dark and illuminated ones by the incident power of 2.72 μW, at V_{ds} = 0 V.

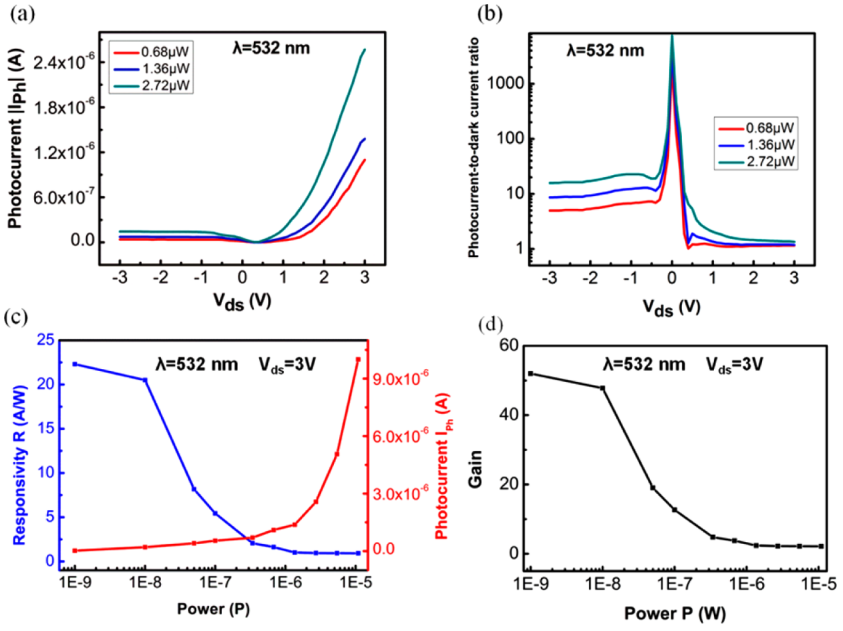

Figure 5. (a) $I_{Ph} - V_{ds}$ curves of the junction under optical irradiation (λ = 532 nm) with various incident laser powers. (b) The on/off ratio between photocurrent I_{Ph} and dark I_{dark} of the junction at the same bias voltage. (c) The photocurrent (I_{Ph}) and photoresponsivity (R) of the junction under optical irradiation (λ = 532 nm) with a series of incident intensities, at V_{ds} = 3 V. (d) The photogain of the junction under optical irradiation (λ = 532 nm) with a series of incident intensities, at V_{ds} = 3 V.

Compared with dark condition, the V_{OC} of the junction has a value of about 0.33 V under green illumination. To explore the photovoltaic effect of the junction, the relationship between the current density and applied voltage is shown in Figure 3b, and the inset schematically describes the separation process of an optically excited exciton occurrence at the heterojunction to be layered-separated electron (e^-) and hole (h^+) carriers. Under green illumination (P_{in}= 2.72 μW), the vertical junction shows a

DOI: 10.1021/acsphotonics.6b00079
ACS Photonics 2016, 3, 692−699

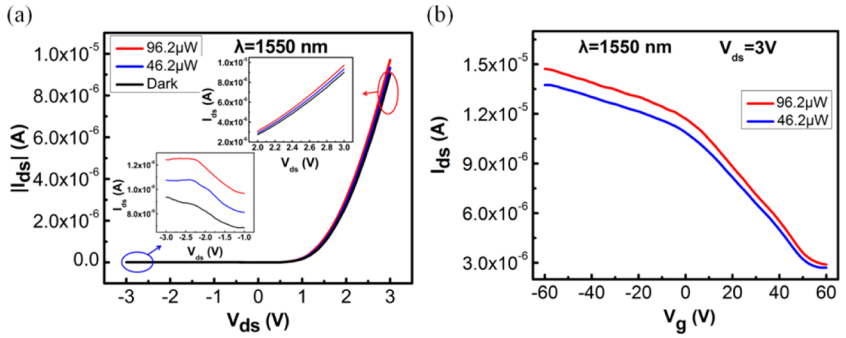

Figure 6. (a) The I–V characteristics of BP/MoS_2 junction under 1.55 μm laser with different incident powers. The top inset shows the I–V details for part of V_{ds} = 2 V to V_{ds} = 3 V, and the bottom inset shows the I–V details for part of from V_{ds} = −3 V to V_{ds} = −1 V. (b) The transfer curves (I–V_g) of the junction under illumination of 1.55 μm laser with different incident powers.

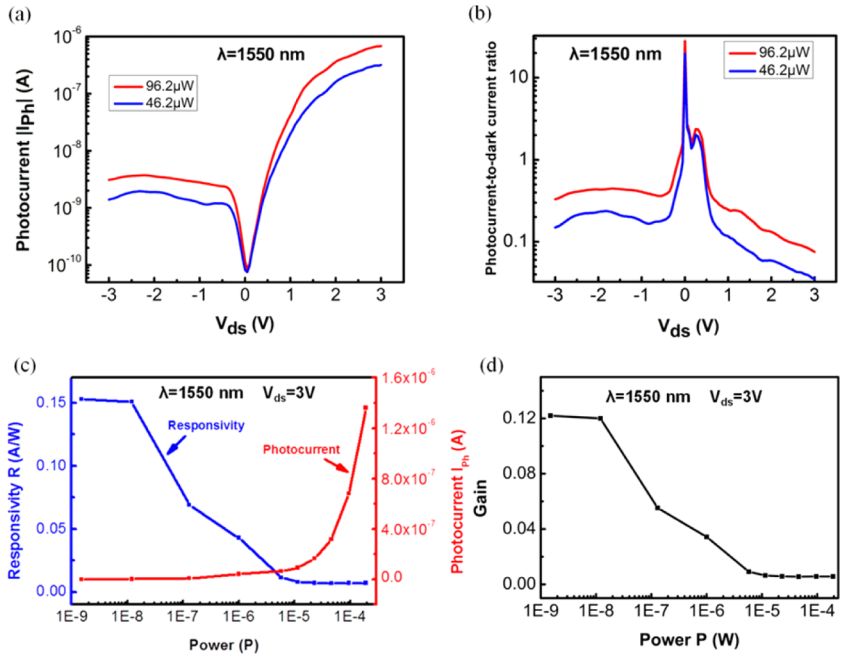

Figure 7. (a) $I_{Ph} - V_{ds}$ curves of the junction under λ = 1.55 μm with various incident laser powers. (b) The on/off ratio between photocurrent I_{Ph} and dark I_{dark} of the junction at the same bias. (c) The photocurrent (I_{Ph}) and photoresponsivity (R) of the junction under λ = 1.55 μm with a series of incident intensities, at V_{ds} = 3 V. (d) The photogain under λ = 1.55 μm with a series of incident intensities, at V_{ds} = 3 V.

photovoltaic response with a V_{OC} of 0.33 V. In addition, the photocurrent density gradually increases with the incident intensity up to near 100 mA cm^{-2}.

Furthermore, the photoresponse characteristics of the BP/MoS_2 heterojunction could also be tuned by varying the gate voltage. The transfer curves (I–V_g) were acquired under illumination with a series of intensities, as shown in Figure 4a. At the applied bias voltage V_{ds} = 1 V, the comparison of I–V curves between the dark and illuminated reveals the current enhancement thanks to the increase in photoinduced carrier. Along with the incident intensity increase, the ambipolar modulation attributed to gate voltage appears more markedly. According to the results, the illuminated transfer characteristics of the heterojunction can be qualitatively viewed as a superposition of the p-type BP and n-type MoS_2 FET transfer characteristics, because of the FET channel consisting of two p- and n-semiconductors in series. Gradually increasing the incident intensity of green laser, the n-type characteristic of the heterojunction becomes more pronounced, leading to the ambipolar transfer characteristics, which indicates the good photoresponsivity of MoS_2 semiconductor for green laser in the heterojunction. Moreover, the short-circuit current (I_{SC}, under V_{ds} = 0) of the junction was measured at the different gate voltage V_g. A representative comparison of the short-circuit current I_{SC} between the dark and illuminated ones with the incident power of 2.72 μW further reveals that the BP/MoS_2 junction generates the photocurrent under illumination, as illustrated in Figure 4b. By varying the gate voltage V_g, there does not exist the short-circuit current across the junction under the dark. However, under illumination, the junction indeed does demonstrate the short-circuit current (I_{SC}). By increasing of gate voltage V_g, the short-circuit current (I_{SC}) under illumination increases to a saturated value after the positive voltage V_g is positively modulated.

Figure 5a shows the I_{Ph}–V_{ds} curves of the junction under optical irradiation (λ = 532 nm) with various incident laser powers. The photocurrent I_{Ph} is defined as $I_{illumination} - I_{dark}$, where $I_{illumination}$ and I_{dark} are the I_{ds} with and without laser illumination, respectively. The positive dependence of the photocurrent I_{Ph} on the incident laser power is presented from

DOI: 10.1021/acsphotonics.6b00079
ACS Photonics 2016, 3, 692–699

the $I_{Ph} - V_{ds}$ results. The on/off ratio is the ratio between photocurrent I_{Ph} and dark I_{dark} of the junction at the same V_{ds}, as shown in Figure 5b. The maximal on/off ratio is about 10^4 at zero-bias voltage, which reveals that the photocurrent is about 4 orders of magnitude higher than the dark current. One of the most important figures of merit for a photodetector is its external photoresponsivity R. Figure 5c shows the photocurrent I_{Ph} and photoresponsivity R acquired at a bias voltage of V_{ds} = 3 V. At low illumination intensity (1 nW), the device reaches a photoresponsivity of 22.3 A W^{-1}, which is about 2 orders of magnitude higher than previously reported values for monolayer MoS_2 phototransistors.[7] We further estimate the photogain to quantify the photosensitivity of the junction. In Figure 5d, the photogain is plotted, which can be calculated by the formula $G = (\Delta I/e)/(P/h\upsilon)$, where ΔI is the photocurrent and P is the incident power. From the result, the photogain in visible region is close to 50, which is comparable to that previously obtained by the photo-field-effect transistors based on III−V semiconductors.[33]

Because of the layer tunable band gap covering the visible to the mid-infrared spectral range, BP can be considered as a potential candidate to apply in broadband optoelectronics. Importantly, due to the finite band gap in BP, the dark current of the BP/MoS_2 heterojunction device is very low. Under the optimal operation conditions (V_g = 60 V, V_{ds} = 1 V), the dark current I_{dark} is only 180 nA, which is more than 3 orders of magnitude less than that of graphene devices under similar conditions, thereby avoiding high Johnson current noise which always plagues graphene-based devices.[34] In Figure 6a, the $I-V$ curves of BP/MoS_2 junction are depicted under illumination by 1.55 μm laser with different incident powers, and the inset shows the detailed $I-V$ curves in a range of V_{ds} from −3 to −1 V and 2 to 3 V, respectively. With incident power increased, the currents I_{ds} demonstrates a appreciable enhancement, indicating that the increase in charge carriers results from the inserted photoinduced carriers of BP. Figure 6b demonstrates the transfer curves ($I-V_g$) of the junction under illumination of 1.55 μm laser with different incident powers. The $I-V_g$ results reveal the typical p-type transfer characteristics. Because of the inability of MoS_2 to absorb the incident 1.55 μm light, the contribution to the current enhancement is dominated by the induced charge carriers from the excitation of BP illuminated by 1.55 μm laser.

The photocurrents ($I_{Ph} = I_{illumination} - I_{dark}$) generated by the heterojunction under illumination of 1.55 μm laser with different incident powers are shown in Figure 7a. Under the optimal conditions (P_{in} = 96.2 μW, V_{ds} = 3 V), the photocurrent generated by the heterojunction with 1.55 μm laser reaches up to 0.7 μA, suggesting that heterojunction structure reliably increases the photoresponsivity of the device. In addition, the on/off ratio of the junction operated under 1.55 μm laser is displayed in Figure 7b. In comparison with the dark current as the background, the photocurrent is 1 order of magnitude higher than background around V_{ds} = 0 V. This indicates that the device has a promising sensitivity in the near-infrared band. The high on/off ratio of the heterojunction is far superior to graphene photodetectors.[35] To further analyze the photoresponsivity of the junction illuminated under 1.55 μm laser, the details of photoresponsivity (R) and photocurrent (I_{Ph}) are demonstrated in Figure 7c. When the illumination intensity is 1 nW and the bias voltage is 3 V, the junction yields the photoresponsivity of 153.4 mA W^{-1}. Moreover, the responsivities and EQE under a spectral illumination (From 532 to 1550 nm) are shown in the Support Information (see Figure S6 and Figure S7). The photogain (Figure 7d) operated under 1.55 μm laser is much lower compared with that operated under 532 nm laser, but this value is still much higher than that achieved by BP photodetector in the photoconductor mode without heterostructure.

The important parameter to quantify the photoresponse property of the detector is the specific detectivity D^* which is calculated by the equation $D^* = (A\Delta f)^{1/2}/\mathrm{NEP}$, where A is the effective area of the detector, Δf is the electrical bandwidth in Hz, and NEP is the noise equivalent power. As the dark current is the major contributor to shot noise, D^* can be expressed as $D^* = I_{Ph}/P(2qAI_{dark})^{1/2}$.[36,37] Based on the measured parameters, the D^* values of the detector are approximately 3.1×10^{11} Jones under 532 nm illumination and 2.13×10^9 Jones under 1550 nm illumination at room temperature.

To explore the application of this BP/MoS_2 heterojunction as photodetector illuminated under 1.55 μm laser, the time-resolved measurement was used to study its photoresponse dynamics. Because the photoexcited carriers must only traverse a distance equal to the depletion width of the junction, the diode-based photodetectors are known for their fast photoresponse times compared with phototransistors. Thus, we demonstrate the dependence of the photosignal on time-response at three different bias voltages, which reveals the rise in photocurrent upon the laser illumination (λ = 1.55 μm) and its decay after laser removal. Indeed, a fast photoresponse for the BP/MoS_2 heterojunction is observed in Figure 8. The

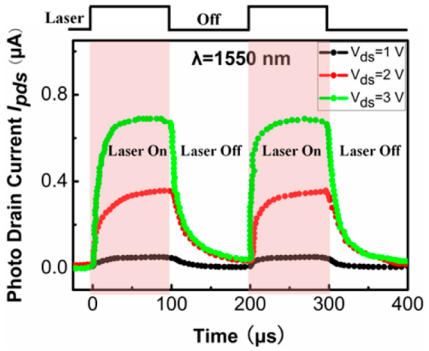

Figure 8. Time-resolved photoresponse of the junction, recorded for different values of bias voltage V_{ds} and P_{in} = 96.2 μW.

response is characterized by a typical rise time of τ_{rise} = 15 μs and τ_{decay} = 70 μs. Importantly, the fast components of the photocurrent rise (τ_{rise}) and decay (τ_{decay}) times reported here are orders of magnitude smaller than those of recently reported heterojunction phototransistors based on graphene.[38−41]

CONCLUSION

In conclusion, we have fabricated a heterojunction diode via a combination of few-layer BP and few-layer MoS_2. The 2D heterojunction diode presents highly electrically gate-tunable current-rectifying $I-V$ characteristics with forward-to-reverse bias current ratios exceeding 10^3. Morevoer, the heterojunction diode serves as a photodetector at near-infrared (λ = 1.55 μm) with the photoresponse of 15 μs, and shows its photoresponsivity of 153.4 mA W^{-1}, which both are a few orders of magnitude better than the reported values of black phosphorus phototransistor. This generic strategy to integrate 2D layered materials in the vertical direction so as to enable functional

DOI: 10.1021/acsphotonics.6b00079
ACS Photonics 2016, 3, 692−699

devices and circuits may open up a new dimension for high-density integration of functional devices in the limited circuit area.

MEHTODS

Device Fabrication. Bulk MoS_2 and black phosphorus were bought from Sigma-Aldrich and Smart-Element, respectively. The few-layer black phosphorus (BP) and few-layer MoS_2 sheets were both mechanically exfoliated using adhesive tape from bulk materials onto the SiO_2 substrate, respectively. Subsequently, the few-layer MoS_2 sheet was transferred onto the few-layer BP sheet to form a 2D BP/MoS_2 heterojunction via van der Waals interaction in the overlapped regions. The electrodes were formed by tailoring 100 nm thick gold film predeposited on another substrate, and then tipped up by a micromanipulator, aligned to the heterojunction and allocated under a 400× optical microscope.

Device Measurement Setup. Devices were measured with a Keithley 4200 semiconductor characterization system. Atomic force microscopy (AFM) image of device was taken in the tapping mode by carrying out on a Nanoscope IIIa Multimode apparatus. Raman spectra of device were obtained using a Raman spectrometer (Renishaw inVia Raman microscope, excitation at 514 nm). SEM images of device were obtained using a field-emission scanning electronmicroscope (Nova NanoSEM 450, FEI) with 10 kV accelerating voltage.

ASSOCIATED CONTENT

Supporting Information

The Supporting Information is available free of charge on the ACS Publications website at DOI: 10.1021/acsphotonics.6b00079.

SEM, SEM EDX mapping, and AFM images, elemental analysis, and $C-V$ characteristics (PDF)

AUTHOR INFORMATION

Corresponding Author

*Fax: +852-2609-8297. Tel: +852-2609-8297. E-mail: jbxu@ee.cuhk.edu.hk.

Author Contributions

‖L.Y. and H.L. contributed equally to this work.

Notes

The authors declare no competing financial interest.

ACKNOWLEDGMENTS

The work is in part supported by Research Grants Council of Hong Kong, particularly, via Grants AoE/P-03/08, N_CUHK405/12, T23-407/13-N, AoE/P-02/12, CUHK1/CRF/12G, and CUHK Group Research Scheme, as well as Innovation and Technology Commission ITS/096/14. J.X. would like to thank the National Science Foundation of China for the support, particularly, via Grant No. 61229401.

REFERENCES

(1) Konstantatos, G.; Sargent, E. H. Solution-Processed Quantum Dot Photodetectors. *Proc. IEEE* **2009**, *97*, 1666−1683.

(2) Rogalski, A.; Antoszewski, J.; Faraone, L. Third-Generation Infrared Photodetector Arrays. *J. Appl. Phys.* **2009**, *105*, 091101−091141.

(3) Konstantatos, G.; Sargent, E. H. Nanostructured Materials for Photon Detection. *Nat. Nanotechnol.* **2010**, *5*, 391−400.

(4) Guo, N.; Hu, W. D.; Liao, L.; Yip, S. P.; Ho, J. C.; Miao, J. S.; Zhang, Z.; Zou, J.; Jiang, T.; Wu, S. W.; Chen, X. S.; Lu, W. Anomalous and Highly Efficient InAs Nanowire Phototransistors Based on Majority Carrier Transport at Room Temperature. *Adv. Mater.* **2014**, *26*, 8203−8209.

(5) Miao, J. S.; Hu, W. D.; Guo, N.; Lu, Z. Y.; Liu, X. Q.; Liao, L.; Chen, P. P.; Jiang, T.; Wu, S. W.; Ho, J. C.; Wang, L.; Chen, X. S.; Lu, W. High-Responsivity Graphene/InAs Nanowire Heterojunction Near-Infrared Photodetection with Distinct Photocurrent on/off Ratios. *Small* **2015**, *11*, 936−942.

(6) Splendiani, A.; Sun, L.; Zhang, Y. B.; Li, T.; Kim, J.; Chim, C. Y.; Galli, G.; Wang, F. Emerging Photoluminescence in Monolayer MoS_2. *Nano Lett.* **2010**, *10*, 1271−1275.

(7) Mak, K. F.; Lee, C.; Hone, J.; Shan, J.; Heinz, T. F. Atomically Thin MoS_2: A New Direct-Gap Semiconductor. *Phys. Rev. Lett.* **2010**, *105*, 136805−136808.

(8) Wang, Q. H.; Kalantar-Zadeh, K.; Kis, A.; Coleman, J. N.; Strano, M. S. Electronics and Optoelectronics of Two-Dimensional Transition Metal Dichalcogenides. *Nat. Nanotechnol.* **2012**, *7*, 699−712.

(9) Wang, X. D.; Wang, P.; Wang, J. L.; Hu, W. D.; Zhou, X. H.; Guo, N.; Huang, H.; Sun, S.; Shen, H.; Lin, T.; Tang, M. H.; Liao, L.; Jiang, A. Q.; Sun, J. L.; Meng, X. J.; Chen, X. S.; Lu, W.; Chu, J. H. Ultrasensitive and Broadband MoS_2 Photodetector Driven by Ferroelectrics. *Adv. Mater.* **2015**, *27*, 6575−6581.

(10) Britnell, L.; Gorbachev, R. V.; Jalil, R. B.; Belle, D.; Schedin, F.; Mishchenko, A.; Georgiou, T.; Katsnelson, M. I.; Eaves, L.; Morozov, S. V.; Peres, N. M. R.; Leist, J.; Geim, A. K.; Novoselov, K. S.; Ponomarenko, L. A. Field-Effect Tunneling Transistor Based on Vertical Graphene Heterostructures. *Science* **2012**, *335*, 947−950.

(11) Georgiou, T.; Jalil, R.; Belle, B. D.; Britnell, L.; Gorbachev, R. V.; Morozov, S. V.; Kim, Y. J.; Gholinia, A.; Haigh, S. J.; Makarovsky, O.; Eaves, L.; Ponomarenko, L. A.; Geim, A. K.; Novoselov, K. S.; Mishchenko, A. Vertical Field-effect Transistor Based on Graphene-WS_2 Heterostructures for Flexible and Transparent Electronics. *Nat. Nanotechnol.* **2013**, *8*, 100−103.

(12) Lopez-Sanchez, O.; Lembke, D.; Kayci, M.; Radenovic, A.; Kis, A. Ultrasensitive Photodectecors Based on Monolayer MoS_2. *Nat. Nanotechnol.* **2013**, *8*, 497−501.

(13) Yin, Z. Y.; Li, H.; Li, H.; Jiang, L.; Shi, Y. M.; Sun, Y. H.; Lu, G.; Zhang, Q.; Chen, X. D.; Zhang, H. Single-Layer MoS_2 Phototransistors. *ACS Nano* **2012**, *6*, 74−80.

(14) Lee, H. S.; Min, S. W.; Chang, Y. G.; Park, M. K.; Nam, T.; Kim, H.; Kim, J. H.; Ryu, S.; Im, S. MoS_2 Nanosheet Phototransistors with Thickness-Modulated Optical Energy Gap. *Nano Lett.* **2012**, *12*, 3695−3700.

(15) Choi, W.; Cho, M. Y.; Konar, A.; Lee, J. H.; Cha, G. B.; Hong, S. C.; Kim, S.; Kim, J.; Jena, D.; Joo, J.; Kim, S. K. High-Detectivity Multilayer MoS2 Phototransistors with Spectral Response from Ultraviolet to Infrared. *Adv. Mater.* **2012**, *24*, 5832−5836.

(16) Ellis, J. K.; Lucero, M. J.; Scuseria, G. E. The Indirect to Direct Band Gap Transition in Multilayered MoS_2 as Predicted by Screened Hybrid Density Functional Theory. *Appl. Phys. Lett.* **2011**, *99*, 261908−261811.

(17) Kang, J.; Tongay, S.; Zhou, J.; Li, J. B.; Wu, J. Q. Band Offsets and Heterostructures of Two-Dimensional Semiconductors. *Appl. Phys. Lett.* **2013**, *102*, 012111−012114.

(18) Yu, W. J.; Liu, Y.; Zhou, H. L.; Yin, A. X.; Li, Z.; Huang, Y.; Duan, X. F. Highly Efficient Gate-Tunable Photocurrent Generation in Vertical Heterostructures of Layered Materials. *Nat. Nanotechnol.* **2013**, *8*, 952−958.

(19) Baugher, B. W. H.; Churchill, H. O. H.; Yang, Y.; Jarillo-Herrero, P. Optoelectronic Devices Based on Electrically Tunable pn Diodes in a Monolayer Dichalcogenides. *Nat. Nanotechnol.* **2014**, *9*, 262−267.

(20) Pospischil, A.; Furchi, M. M.; Mueller, T. Solar-Energy Conversion and Light Emission in an Atomic Monolayer pn Diode. *Nat. Nanotechnol.* **2014**, *9*, 257−261.

(21) Ross, J. S.; Klement, P.; Jones, A. M.; Ghimire, N. J.; Yan, J. Q.; Mandrus, D. G.; Taniguchi, T.; Watanabe, K. J.; Kitamura, K. J.; Yao,

DOI: 10.1021/acsphotonics.6b00079
ACS Photonics 2016, 3, 692−699

W.; Cobden, D. H.; Xu, X. D. Electrically Tunable Excitonic Light-Emitting Diodes Based on Monolayer WSe_2 pn Junctions. *Nat. Nanotechnol.* **2014**, *9*, 268−272.
(22) Buscema, M.; Groenendijk, D. J.; Steele, G. A.; van der Zant, H. S. J.; Castellanos-Gomez, A. Photovoltaic Effect in Few-Layer Black Phosphorus pn Junctions Defined by Local Electrostatic Gating. *Nat. Commun.* **2014**, *5*, 4651−4657.
(23) Buscema, M.; Groenendijk, D. J.; Blanter, S. I.; Steele, G. A.; van der Zant, H. S. J.; Castellanos-Gomez, A. Fast and Broadband Photoresponse of Few-Layer Black Phosphorus Field-effect Transistors. *Nano Lett.* **2014**, *14*, 3347−3352.
(24) Baugher, B. W. H.; Churchill, H. O. H.; Yang, Y.; Jarillo-Herrero, P. Optoelectronic Devices Based on Electrically Tunable pn Diodes in a Monolayer Dichalcogenides. *Nat. Nanotechnol.* **2014**, *9*, 262−267.
(25) Liu, H.; Neal, A. T.; Zhu, Z.; Luo, Z.; Xu, X.; Tomanek, D.; Ye, P. D. Phosphorene: An Unexplored 2D Semiconductor with A High Hole Mobility. *ACS Nano* **2014**, *8*, 4033−4041.
(26) Najmaei, S.; Liu, Z.; Zhou, W.; Zou, X.; Shi, G.; Lei, S.; Yakobson, B. I.; Idrobo, J. C.; Ajayan, P. M.; Lou, J. Vapour Phase Growth and Grain Boundary Structure of Molybdenum Disulphide Atomic Layers. *Nat. Mater.* **2013**, *12*, 754−759.
(27) Shah, J. M.; Li, Y. L.; Gessmann, T.; Schubert, E. F. Experimental Analysis and Theoretical Model for Anomalously High Ideality Factors (n≫2.0) in AlGaN/GaN pn Junction Diodes. *J. Appl. Phys.* **2003**, *94*, 2627−2630.
(28) Cheng, R.; Li, D. H.; Zhou, H. L.; Wang, C.; Yin, A. X.; Jiang, S.; Liu, Y.; Chen, Y.; Huang, Y.; Duan, X. F. Electroluminescence and Photocurrent Generation from Atomically Sharp WSe_2/MoS_2 Heterojunction p-n Diodes. *Nano Lett.* **2014**, *14*, 5590−5597.
(29) Yu, W. J.; Li, Z.; Zhou, H. L.; Chen, Y.; Wang, Y.; Huang, Y.; Duan, X. F. Vertically Stacked Multi-Heterostructures of Layered Materials for Logic Transistors and Complementary Inverters. *Nat. Mater.* **2013**, *12*, 246−252.
(30) Jariwala, D.; Sangwan, V. K.; Wu, C. C.; Prabhumirashi, P. L.; Geier, M. L.; Marks, T. J.; Lauhon, L. J.; Hersam, M. C. Gate-Tunable Carbon Nanotube-MoS_2 Heterojunction p-n Diode. *Proc. Natl. Acad. Sci. U. S. A.* **2013**, *110*, 18076−18080.
(31) Tran, V.; Soklaski, R.; Liang, Y. F.; Yang, L. Layer-Controlled Band Gap and Anisotropic Excitons in Few-layer Black Phosphorus. *Phys. Rev. B: Condens. Matter Mater. Phys.* **2014**, *89*, 235319−235325.
(32) Yin, Z.; Li, H.; Li, H.; Jiang, L.; Shi, Y.; Sun, Y. H.; Lu, G.; Zhang, Q.; Chen, X. D.; Zhang, H. Single-Layer MoS_2 Phototransistors. *ACS Nano* **2012**, *6*, 74−80.
(33) Ogura, M. Hole Injection Type InGaAs−InP Near Infrared Photo-FET (HI-FET). *IEEE J. Quantum Electron.* **2010**, *46*, 562−569.
(34) Freitag, M.; Low, T.; Xia, F. N.; Avouris, P. Photoconductivity of Biased Graphene. *Nat. Photonics* **2013**, *7*, 53−59.
(35) Mueller, T.; Xia, F. N.; Avouris, P. Graphene Photodetectors for High-Speed Optical Communications. *Nat. Photonics* **2010**, *4*, 297−301.
(36) Zhang, W.; Chiu, M. H.; Chen, C. H.; Chen, W.; Li, L. J.; Wee, A. T. S. Role of Metal Contacts in High-Performance Phototransistors Based on WSe_2 Monolayers. *ACS Nano* **2014**, *8*, 8653−8661.
(37) Manga, K. K.; Wang, S.; Jaiswal, M.; Bao, Q. L.; Loh, K. P. High-Gain Graphene-Titanium Oxide Photoconductor Made from Inkjet Printable Ionic Solution. *Adv. Mater.* **2010**, *22*, 5265−5270.
(38) Gan, X.; Shiue, R. J.; Gao, Y.; Meric, I.; Heinz, T. F.; Shepard, K.; Hone, J.; Assefa, S.; Englund, D. Chip-Integrated Ultrafast Graphene Photodetector with High Responsivity. *Nat. Photonics* **2013**, *7*, 883−887.
(39) Xia, F.; Mueller, T.; Lin, Y.-m.; Valdes-Garcia, A.; Avouris, P. Ultrafast Graphene Photodetector. *Nat. Nanotechnol.* **2009**, *4*, 839−843.
(40) Konstantatos, G.; Badioli, M.; Gaudreau, L.; Osmond, J.; Bernechea, M.; de Arquer, F. P. G.; Gatti, F.; Koppens, F. H. L. Hybrid Graphene-Quantum Dot Phototransistors with Ultrahigh Gain. *Nat. Nanotechnol.* **2012**, *7*, 363−368.
(41) Roy, K.; Padmanabhan, M.; Goswami, S.; Sai, T. P.; Ramalingam, G.; Raghavan, S.; Ghosh, A. Graphene-MoS_2 Hybrid Structures for Multifunctional Photoresponsive Memory Devices. *Nat. Nanotechnol.* **2013**, *8*, 826−830.

DOI: 10.1021/acsphotonics.6b00079
ACS Photonics 2016, 3, 692−699